Inorg. Chem. **2008**, *47*, 7106−7113

Redox Properties of Ruthenium Nitrosyl Porphyrin Complexes with Different Axial Ligation: Structural, Spectroelectrochemical (IR, UV−Visible, and EPR), and Theoretical Studies

Priti Singh,[†] Atanu Kumar Das,[†] Biprajit Sarkar,[†] Mark Niemeyer,[†] Federico Roncaroli,[‡] José A. Olabe,[‡] Jan Fiedler,[§] Stanislav Záliš,[§] and Wolfgang Kaim*[,†]

Institut für Anorganische Chemie, Universität Stuttgart, Pfaffenwaldring 55, D-70550 Stuttgart, Germany, Departamento de Química Inorgánica, Analítica y Química Física and INQUIMAE, Facultad de Ciencias Exactas y Naturales, UBA, Pabellón 2, Ciudad Universitaria, C1428EHA Buenos Aires, Republic of Argentina, and J. Heyrovský Institute of Physical Chemistry, v.v.i., Academy of Sciences of the Czech Republic, Dolejškova 3, CZ-18223 Prague, Czech Republic

Received December 5, 2007

Experimental and computational results for different ruthenium nitrosyl porphyrin complexes $[(Por)Ru(NO)(X)]^{n+}$ (where Por^{2-} = tetraphenylporphyrin dianion (TPP^{2-}) or octaethylporphyrin dianion (OEP^{2-}) and X = H_2O (n = 1, 2, 3) or pyridine, 4-cyanopyridine, or 4-*N,N*-dimethylaminopyridine (n = 1, 0)) are reported with respect to their electron-transfer behavior. The structure of $[(TPP)Ru(NO)(H_2O)]BF_4$ is established as an $\{MNO\}^6$ species with an almost-linear RuNO arrangement at 178.1(3)°. The compound $[(Por)Ru(NO)(H_2O)]BF_4$ undergoes two reversible one-electron oxidation processes. Spectroelectrochemical measurements (IR, UV−vis−NIR, and EPR) indicate that the first oxidation occurs on the porphyrin ring, as evident from the appearance of diagnostic porphyrin radical-anion vibrational bands (1530 cm^{-1} for $OEP^{\bullet-}$ and 1290 cm^{-1} for $TPP^{\bullet-}$), from the small shift of ∼20 cm^{-1} for ν_{NO} and from the EPR signal at $g_{iso} \approx 2.00$. The second oxidation, which was found to be electrochemically reversible for the OEP compound, shows a 55 cm^{-1} shift in ν_{NO}, suggesting a partially metal-centered process. The compounds $[(Por)Ru(NO)(X)]BF_4$, where X = pyridines, undergo a reversible one-electron reduction. The site of the reduction was determined by spectroelectrochemical studies to be NO-centered with a ca. −300 cm^{-1} shift in ν_{NO}. The EPR response of the $NO^{\bullet}$ complexes was essentially unaffected by the variation in the substituted pyridines X. DFT calculations support the interpretation of the experimental results because the HOMO of $[(TPP)Ru(NO)(X)]^+$, where X = H_2O or pyridines, was calculated to be centered at the porphyrin π system, whereas the LUMO of $[(TPP)Ru(NO)(X)]^+$ has about 50% π^*(NO) character. This confirms that the (first) oxidation of $[(Por)Ru(NO)(H_2O)]^+$ occurs on the porphyrin ring wheras the reduction of $[(Por)Ru(NO)(X)]^+$ is largely NO-centered with the metal remaining in the low-spin ruthenium(II) state throughout. The 4% pyridine contribution to the LUMO of $[(TPP)Ru(NO)(py)]^+$ is correlated with the stability of the reduced form as opposed to that of the aqua complex.

Introduction

The interaction of nitric oxide with heme proteins plays a very important role in many physiological processes.[1,2] Nitric oxide is biosynthesized by a class of enzymes called nitric oxide synthases (NOSs),[2a] which contain heme as a prosthetic group. Soluble guanylate cyclase (sGC) is one of the other heme-containing enzymes that act as biological receptors for NO.[2b] In addition to its significance in physiology, the interaction of NO with heme is also important in the nitrogen cycle.[2c] Because of the general importance of the heme−NO interaction, a large amount of research has been carried out toward the synthesis of corresponding model systems. These investigations employ synthetic porphyrins such as tetraphenylporphyrin (TPP) or the more electron-rich octaethylpor-

* Corresponding author: E-mail. kaim@iac.uni-stuttgart.de.
[†] Universität Stuttgart.
[‡] Universidad de Buenos Aires.
[§] Academy of Sciences of the Czech Republic.

10.1021/ic702371t CCC: $40.75
Published on Web 07/23/2008

phyrin (OEP), and iron nitrosyl complexes of these synthetic porphyrins have been extensively studied.[3] Many investigations on iron nitrosyl porphyrins have included variations of the axial ligand in the trans position to NO, ranging from N donors,[3c,d] such as pyridine, imidazole, or piperidine, to S donors, such as thiolates,[3e,h] in order to understand the role of axial ligands in the properties of coordinated NO.

The heavier analogues of iron, ruthenium nitrosyl porphyrins, have also been anticipated to be promising models in the study of the interactions of NO with heme because of their enhanced stability relative to iron nitrosyl complexes.[4] However, in contrast to the several reports on the syntheses[4c,d,5] and structural studies[6] of ruthenium nitrosyl porphyrins, there have been far fewer investigations on the electrochemistry[7] and spectroelectrochemistry[8,9] of ruthenium nitrosyl porphyrins despite the fact that these would be essential in understanding electron-transfer processes. In addition, the unambiguous assignment of the NO oxidation state[10] for NO-coordinated ruthenium porphyrin complexes [(Por)Ru(NO)(X)] with different porphyrins (Por) and various axial ligands (X) can be useful in understanding the electron-transfer processes. All three components, the porphinato ligands ($Por^{-/2-/3-}$), the metal ($Ru^{2+/3+}$), and the NO system ($NO^{+/0/-}$) are redox-active in the central redox potential region so that the determination of individual oxidation state combinations is not trivial.

In this Article, we report experimental and theoretical studies of two different ruthenium nitrosyl porphyrin complexes in which we vary the axial ligand from an aqua ligand to acceptor- or donor-substituted pyridines. The effect of axial ligands on the redox properties of ruthenium nitrosyl porphyrin complexes has been investigated by means of electrochemical and various spectroelectrochemical methods, including EPR. In a recent report, the small variance in EPR parameters for very different compounds containing the $\{RuNO\}^7$ configuration was noted.[11]

Experimental Section

Instrumentation. EPR spectra in the X band were recorded with a Bruker System EMX. IR spectra were obtained using a Nicolet 6700 FT-IR instrument; solid-state IR measurements were performed with an ATR unit (smart orbit with diamond crystal). UV−vis−NIR absorption spectra were recorded on J&M TIDAS and Shimadzu UV 3101 PC spectrophotometers. Cyclic voltammetry was carried out in 0.1 M Bu_4NClO_4 solutions using a three-electrode configuration (glassy carbon working electrode, Pt counter electrode, and Ag wire as a pseudoreference) and a PAR 273 potentiostat and function generator. The ferrocene/ferrocenium (Fc/Fc^+) couple served as an internal reference. Spectroelectrochemistry was performed by our use of an optically transparent low-temperature cell.[12a] A two-electrode capillary served to generate intermediates for X-band EPR studies.[12b]

Synthesis. The complex $[(TPP)Ru(NO)(H_2O)]BF_4$ was prepared according to the literature[7a] and was additionally characterized by single-crystal X-ray crystallography. The complex $[(OEP)Ru(NO)(H_2O)]BF_4$ was prepared according to the literature.[13] The reduction studies for $[(TPP)Ru(NO)(X)]BF_4$ and $[(OEP)Ru(NO)(X)]BF_4$, where X = pyridine, 4-cyanopyridine, or 4-*N,N*-dimethylaminopyridine, were performed after an electrocatalyzed exchange in a solution of the aqua complex in an excess (ca. 10-fold) of the respective pyridine.[7]

X-ray Structure Determination of $[(TPP)Ru(NO)(H_2O)]BF_4 \cdot 2H_2O$. Dark-red crystals were grown by the slow diffusion of hexane into a dichloromethane solution at 269 K. A suitable crystal

(1) (a) Murad, F. *Angew. Chem., Int. Ed.* **1999**, *28*, 1856. (b) Ribiero, J. M. C.; Hazzard, J. M. H.; Nussenzveig, R. H.; Champagne, D. E.; Walker, F. A. *Science* **1993**, *260*, 539. (c) *Methods in Nitric Oxide Research*; Feelisch, M., Stamler, J. S., Eds.; Wiley: Chichester, U.K., 1996. (d) Wang, P. G.; Xian, M.; Tang, X.; Wu, X.; Wen, Z.; Cai, T.; Janczuk, A. *Chem. Rev.* **2002**, *102*, 1091. (e) Hrabie, J. A.; Keefer, L. K. *Chem. Rev.* **2002**, *102*, 1135. (f) *Nitric Oxide Donors: For Pharmaceutical and Biological Applications*; Wang, P. G., Cai, T. B., Taniguchi, N., Eds.; Wiley-VCH: Weinheim, Germany, 2005. (g) Ford, P. C.; Laverman, L. E.; Lorkovic, I. M. *Adv. Inorg. Chem.* **2003**, *51*, 203. (h) Cheng, L.; Richter-Addo, G. B. Binding and Activation of Nitric Oxide by Metalloporphyrins and Heme. In *The Porphyrin Handbook*; Guilard, R., Smith, K. M., Kadish, K. M., Eds.; Academic Press: New York, 2000; *Vol. 4*, Chapter 33.

(2) (a) Alderton, W. K.; Cooper, C. E.; Knowles, R. G. *Biochem. J.* **2001**, *357*, 593. (b) Boon, E. M.; Huang, S. H.; Marletta, M. A. *Nat. Chem. Biol.* **2005**, *1*, 53. (c) Averill, B. A. *Chem. Rev.* **1996**, *96*, 2951. (d) Tocheva, E. I.; Rosell, F. I.; Mauk, A. G.; Murphy, M. E. P. *Science* **2004**, *304*, 867. (e) Aboelella, N. W.; Reynolds, A. M.; Tolman, W. B. *Science* **2004**, *304*, 836.

(3) (a) Ford, P. C.; Lorkovic, I. M. *Chem. Rev.* **2002**, *102*, 993. (b) Praneeeth, V. K. K.; Neese, F.; Lehnert, N. *Inorg. Chem.* **2005**, *44*, 2570. (c) Wyllie, G. R. A.; Schulz, C. E.; Scheidt, W. R. *Inorg. Chem.* **2003**, *42*, 5722. (d) Praneeth, V. K. K.; Näther, C.; Peters, G.; Lehnert, N. *Inorg. Chem.* **2006**, *45*, 2795. (e) Praneeth, V. K. K.; Haupt, E.; Lehnert, N. *Inorg. Biochem.* **2005**, *99*, 940. (f) Novozhilova, I. V.; Philip, C.; Lee, J.; Richter-Addo, G. B.; Bagley, K. A. *J. Am. Chem. Soc.* **2006**, *128*, 2093. (g) Richter-Addo, G. B.; Wheeler, R. A.; Hixson, C. A.; Chen, L.; Khan, M. A.; Ellison, M. A.; Schulz, C. E.; Scheidt, W. R. *J. Am. Chem. Soc.* **2001**, *123*, 6314. (h) Paulat, F.; Lehnert, N. *Inorg. Chem.* **2007**, *46*, 1547.

(4) (a) Ford, P. C.; Laverman, L. E. *Coord. Chem. Rev.* **2005**, *249*, 391. (b) ¸Zanichelli, P. G.; Miotto, A. M.; Estrela, H. F. G.; Soares, F. R.; Grasi-Kassisse, D. M.; Spadari-Bratfisch, R. C.; Castellano, E. E.; Roncaroli, F.; Parise, A. R.; Olabe, J. A.; de Brito, A. R. M. S.; Franco, D. W. *Inorg. Biochem.* **2004**, *98*, 1921. (c) Miranda, K. M.; Bu, X.; Lorkovi, I.; Ford, P. C. *Inorg. Chem.* **1997**, *36*, 4838. (d) Bohle, D. S.; Hung, C. H.; Smith, B. D. *Inorg. Chem.* **1998**, *37*, 5798.

(5) Antipas, A.; Buchler, J. W.; Gouterman, M.; Smith, P. D. *J. Am. Chem. Soc.* **1978**, *100*, 3015.

(6) (a) Wyllie, G. R. A.; Scheidt, W. R. *Chem. Rev.* **2002**, *102*, 1067. (b) Bezerra, C. W. B.; da Silva, S. C.; Gambardella, M. T. P.; Santos, R. H. A.; Plicas, L. M. A.; Tfouni, E.; Franco, D. W. *Inorg. Chem.* **1999**, *38*, 5660. (c) Tfouni, E.; Krieger, M.; McGarvey, B. R.; Franco, D. W. *Coord. Chem. Rev.* **2003**, *236*, 57.

(7) (a) Kadish, K. M.; Adamian, V. A.; Van Caemelbecke, E.; Tan, Z.; Tagliatesta, P.; Bianco, P.; Boschi, T.; Yi, G.-B.; Khan, M. A.; Richter-Addo, G. B. *Inorg. Chem.* **1996**, *35*, 1343. (b) Kadish, K. M. *Prog. Inorg. Chem.* **1986**, *34*, 435.

(8) Carter, C. M.; Lee, J.; Hixson, C. A.; Powell, D. R.; Wheeler, R. A.; Shaw, M. J.; Richter-Addo, G. B. *Dalton Trans.* **2006**, 1338.

(9) (a) Brown, G. M.; Hopf, F. R.; Ferguson, J. A.; Meyer, T. J.; Whitten, D. G. *J. Am. Chem. Soc.* **1973**, *95*, 5939. (b) Kadish, K. M.; Mu, X. *Pure Appl. Chem.* **1990**, *62*, 1051. (c) Mu, X. H.; Kadish, K. M. *Langmuir* **1990**, *6*, 51. (d) Rillema, D. P.; Nagle, J. K.; Barrringer, L. F.; Meyer, T. J. *J. Am. Chem. Soc.* **1981**, *103*, 56. (e) Morishima, I.; Takamuki, Y.; Shiro, Y. *J. Am. Chem. Soc.* **1984**, *106*, 7666. (f) Fujita, E.; Chang, C. K.; Fajer, J. *J. Am. Chem. Soc.* **1985**, *107*, 7665.

(10) (a) McCleverty, J. A. *Chem. Rev.* **2004**, *104*, 403. (b) Enemark, J. H.; Feltham, R. D. *Coord. Chem. Rev.* **1974**, *13*, 339. (c) Westcott, B. L.; Enemark, J. H. In *Inorganic Electronic Structure and Spectroscopy*; Solomon, E. I., Lever, A. B. P., Eds.; Wiley: New York, 1999; Vol. *2*, p 403.

(11) Frantz, S.; Sarkar, B.; Sieger, M.; Kaim, W.; Roncaroli, F.; Olabe, J. A.; Záliš, S. *Eur. J. Inorg. Chem.* **2004**, 2902, and literature cited.

(12) (a) Mahabiersing, T.; Luyten, H.; Nieuwendam, R. C.; Hartl, F. *Collect. Czech. Chem. Commun.* **2003**, *68*, 1687. (b) Kaim, W.; Ernst, S.; Kasack, V. *J. Am. Chem. Soc.* **1990**, *112*, 173.

(13) Yi, G.; Khan, M. A.; Richter-Addo, G. B. *Inorg. Chem.* **1996**, *35*, 3453.

(14) (a) Hope, H. *Prog. Inorg. Chem.* **1995**, *41*, 1. (b) Sheldrick G. M. *SHELXTL*, PC 5.03; Siemens Analytical X-ray Instruments Inc.: Madison, WI, 1994. (c) Sheldrick, G. M. *Program for Crystal Structure Solution and Refinement*; Universität Göttingen, 1997.

Table 1. Crystallographic Data for $[(TPP)Ru(NO)(H_2O)]BF_4 \cdot 2H_2O$

empirical formula	$C_{44}H_{30}BF_4N_5O_4Ru$
fw	880.61
T (K)	173(2)
λ (Å)	0.71073
cryst syst	monoclinic
space group	$P2_1/n$
Z	4
a (Å)	15.558(3)
b (Å)	15.255(3)
c (Å)	17.567(3)
β (deg)	93.355(14)
V (Å^3)	4162.3(12)
ρ_{calcd} (g·cm^{-3})	1.405
μ (mm^{-1})	0.443
2θ range (deg)	3−53
collected data	8952
unique data/R_{int}	8632/0.029
no. of data $>2\sigma$	6155
no. of parameters	569
GOF[a]	0.975
R1, wR2 ($I > 2\sigma$)[b]	0.0437, 0.1151
R1, wR2 (all data)[b]	0.0645, 0.1205
resd dens (e/Å^3)	0.999/−0.902

[a] GOF = $\{\sum[w(F_o^2 - F_c^2)^2]/(n-p)\}^{1/2}$, where n and p denote the number of data and parameters. [b] R1 = $\sum(||F_o| - |F_c||)/\sum|F_o|$ and wR2 = $\{\sum[w(F_o^2 - F_c^2)^2]/\sum[w(F_o^2)^2]\}^{1/2}$ where $w = 1/[\sigma^2(F_o^2) + (aP)^2 + bP]$ and $P = [(\max; 0, F_o^2) + 2F_c^2]/3$.

was selected under a layer of viscous hydrocarbon oil, attached to a glass fiber, and instantly placed in a low-temperature N_2 stream.[14a] The X-ray intensity data were collected at 173 K using a Siemens P4 diffractometer. Crystal data are given in Table 1. Calculations were performed with the SHELXTL PC 5.03[14b] and SHELXL-97[14c] program systems installed on a local PC. The structures were solved by direct methods and refined on F_o^2 by full-matrix least-squares refinement. An absorption correction was applied by using semiempirical ψ scans. Anisotropic thermal parameters were included for all nonhydrogen atoms. The disordered BF_4 anion was refined with split positions and a side occupation factor of 0.50. The B−F distances were restrained with SADI commands. Hydrogen atoms on the coordinated water molecule were allowed to refine freely, whereas hydrogen atoms on the two cocrystallized water molecules could not be located. Final R values are listed in Table 1. Important bond parameters are given in Table S1.

DFT Calculations. The electronic structures of all complexes were calculated by density functional theory (DFT) methods using the Gaussian 03[15a] and ADF2006.01[15b,c] program packages. To simplify some of the calculations, the ethyl substituent was replaced by methyl in $[(OEP)Ru(NO)(H_2O)]^n$, leading to $[(OMP)Ru(NO)(H_2O)]^n$. The calculations of the vibrational frequencies were performed at optimized geometries. Low-lying excited states were calculated by the time-dependent DFT (TD-DFT) method.

The hybrid functional of Perdew, Burke, and Ernzerhof[16a] (PBE0) was used within Gaussian (G03/PBE0) with 6-31G* polarized double-ζ basis sets[16b] for C, N, H, and O atoms and effective core pseudopotentials and with corresponding optimized sets of basis functions for Ru atoms.[16c] During the geometry optimization of the complex $[(TPP)Ru(NO)(H_2O)]^+$ the triple-ζ basis augmented by diffuse functions (aug-cc-pvtz)[16d] was used for O within the H_2O ligand. The vibrational analysis was done with the "pure" density functional BPW91.[16e,f] The polarizable conductor calculation model (CPCM) was used for the modeling of the solvent influence in TD-DFT calculations.

Slater type orbital (STO) basis sets of triple-ζ quality with two polarization functions for the Ru atom and of triple-ζ quality with one polarization function for the remaining atoms were employed in ADF2006.01. The inner shells were represented by the frozen core approximation (1s for C, N, and O and 1s−3d for Ru were kept frozen). The calculations were performed with the functional including Becke's gradient correction[16e] to the local exchange expression in conjunction with Perdew's gradient correction[16g] to the local correlation (ADF/BP). The scalar relativistic (SR) zeroth-order regular approximation (ZORA) was used within ADF calculations. The **g** tensor was obtained from a spin-nonpolarized wave function after incorporating the spin−orbit (SO) coupling. **A** and **g** tensors were obtained by first-order perturbation theory from a ZORA Hamiltonian in the presence of a time-independent magnetic field.[17a,b] Core electrons were included in calculations of **A** tensors.

Results and Discussion

Crystal Structure. The complex $[(TPP)Ru(NO)(H_2O)]BF_4$ was synthesized by a reported method[7a] and characterized additionally by X-ray crystallography (Table 1, Figure 1). The molecular structure in the crystal confirms the $\{RuNO\}^6$ configuration[10b] as $[(TPP^{2-})Ru^{II}(NO^+)(H_2O)]BF_4$ via the nearly linear (178.1(3)°) RuNO arrangement (Figure 1, Table S1) and the typical[6,10,18] Ru−N (1.726(3) Å) and N−O (1.143(4) Å) bond lengths. The experimental geometry is reasonably described by DFT calculations, as shown in Table S1. Both G03/PBE0 and ADF/BP methods yield an almost linear Ru−N−O bond. Wheras the calculations overestimate the Ru−H_2O distance, the Ru−N bond lengths are reproduced within 0.02 Å. The calculations with the 6-31G* double-ζ basis resulted in Ru−O bonds that were too long, but after adding diffuse functions and enlarging the basis set, the calculated Ru−O bond length converged to the experimental value.

Cyclic Voltammetry. Cyclic voltammetry has been employed in the study of the precursor compounds [(TPP)-

(15) (a) Frisch, M. J.; Trucks, G. W.; Schlegel, H. B.; Scuseria, G. E.; Robb, M. A.; Cheeseman, J. R.; Montgomery, J. A., Jr.; Vreven, T.; Kudin, K. N.; Burant, J. C.; Millam, J. M.; Iyengar, S. S.; Tomasi, J.; Barone, V.; Mennucci, B.; Cossi, M.; Scalmani, G.; Rega, N.; Petersson, G. A.; Nakatsuji, H.; Hada, M.; Ehara, M.; Toyota, K.; Fukuda, R.; Hasegawa, J.; Ishida, M.; Nakajima, T.; Honda, Y.; Kitao, O.; Nakai, H.; Klene, M.; Li, X.; Knox, J. E.; Hratchian, H. P.; Cross, J. B.; Bakken, V.; Adamo, C.; Jaramillo, J.; Gomperts, R.; Stratmann, R. E.; Yazyev, O.; Austin, A. J.; Cammi, R.; Pomelli, C.; Ochterski, J. W.; Ayala, P. Y.; Morokuma, K.; Voth, G. A.; Salvador, P.; Dannenberg, J. J.; Zakrzewski, V. G.; Dapprich, S.; Daniels, A. D.; Strain, M. C.; Farkas, O.; Malick, D. K.; Rabuck, A. D.; Raghavachari, K.; Foresman, J. B.; Ortiz, J. V.; Cui, Q.; Baboul, A. G.; Clifford, S.; Cioslowski, J.; Stefanov, B. B.; Liu, G.; Liashenko, A.; Piskorz, P.; Komaromi, I.; Martin, R. L.; Fox, D. J.; Keith, T.; Al-Laham, M. A.; Peng, C. Y.; Nanayakkara, A.; Challacombe, M.; Gill, P. M. W.; Johnson, B.; Chen, W.; Wong, M. W.; Gonzalez, C.; Pople, J. A. *Gaussian 03*, revision C.02; Gaussian, Inc.: Wallingford, CT, 2004. (b) te Velde, G.; Bickelhaupt, F. M.; van Gisbergen, S. J. A.; Fonseca Guerra, C.; Baerends, E. J.; Snijders, J. G.; Ziegler, T. *J. Comput. Chem.* **2001**, *22*, 931. (c) *ADF2006.01*;Theoretical Chemistry, Vrije Universiteit: Amsterdam, 2006, http://www.scm.com.

(16) (a) Perdew, J. P.; Burke, K.; Ernzerhof, M. *Phys. Rev. Lett.* **1996**, *77*, 3865. (b) Hariharan, P. C.; Pople, J. A. *Theor. Chim. Acta* **1973**, *28*, 213. (c) Andrae, D.; Häussermann, U.; Dolg, M.; Stoll, H.; Preuss, H. *Theor. Chim. Acta* **1990**, *77*, 123. (d) Woon, D. E.; Dunning, T. H., Jr. *J. Chem. Phys.* **1995**, *103*, 4572. (e) Becke, A. D. *Phys. Rev. A* **1988**, *38*, 3098. (f) Perdew, J. P.; Wang, Y. *Phys. Rev. B* **1992**, *45*, 13244. (g) Perdew, J. P. *Phys. Rev. B* **1986**, *33*, 8822.

(17) (a) van Lenthe, E.; van der Avoird, A.; Wormer, P. E. S. *J. Chem. Phys.* **1997**, *107*, 2488. (b) van Lenthe, E.; van der Avoird, A.; Wormer, P. E. S. *J. Chem. Phys.* **1998**, *108*, 4783.

(18) Scheidt, W. R.; Ellison, M. K. *Acc. Chem. Res.* **1999**, *32*, 350.

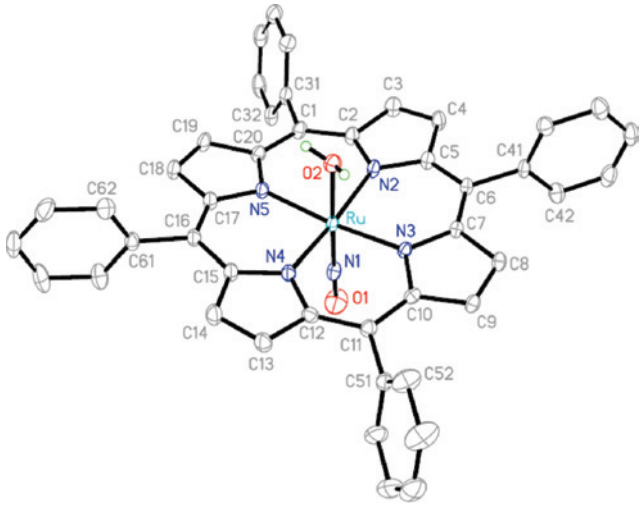

Figure 1. Molecular structure of the cation in the crystal of $[(TPP)Ru(NO)(H_2O)]BF_4 \cdot 2H_2O$ at 173 K.

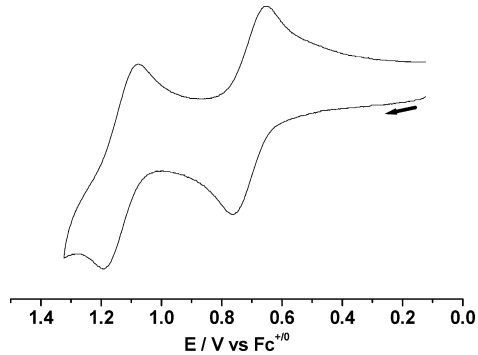

Figure 2. Cyclic voltammogram of $[(OEP)Ru(NO)(H_2O)]BF_4$ in CH_2Cl_2/0.1 M n-Bu_4NClO_4 at 25 °C (oxidation); scan rate = 200 mV/s.

Table 2. Redox Potentials of Complexes[a]

complex	$E_{1/2}$(ox1)	$E_{1/2}$(ox2)	$E_{1/2}$(red1)
$[(TPP)Ru(NO)(H_2O)]BF_4$	0.78	1.14[c]	*b*
$[(TPP)Ru(NO)(py)]BF_4$	*b*	n.o.	−0.79
$[(TPP)Ru(NO)(4\text{-CN-py})]BF_4$	*b*	n.o.	−0.68
$[(TPP)Ru(NO)(4\text{-}N,N\text{-}Me_2N\text{-py})]BF_4$	*b*	n.o.	−0.90
$[(OEP)Ru(NO)(H_2O)]BF_4$	0.71	1.13	*b*
$[(OEP)Ru(NO)(py)]BF_4$	*b*	n.o.	−0.95
$[(OEP)Ru(NO)(4\text{-CN-py})]BF_4$	*b*	n.o.	−0.67
$[(OEP)Ru(NO)(4\text{-}N,N\text{-}Me_2N\text{-py})]BF_4$	*b*	n.o.	−1.00

[a] Potentials in volts versus $[Fe(C_5H_5)_2]^{+/0}$ from cyclic voltammetry at 100 mV/s in CH_2Cl_2/0.1 M Bu_4NClO_4 solutions. [b] Irreversible process. [c] Only partially reversible.

$Ru(NO)(H_2O)]^+$ and $[(OEP)Ru(NO)(H_2O)]BF_4$ and the analogues containing pyridines instead of H_2O in the trans position to NO. The exchange could be affected electrocatalytically by setting the working electrode potential to ca. 200 mV before the cathodic peak maximum (Figure S1). A cyclic voltammogram for the oxidation of $[(OEP)Ru(NO)(H_2O)]^+$ in CH_2Cl_2/0.1 M n-Bu_4NClO_4 is shown in Figure 2. The compound undergoes two one-electron reversible oxidation processes at $E_{1/2}$(ox1) = 0.71 V and $E_{1/2}$(ox2) = 1.13 V versus $Fc^{+/0}$. The redox potentials shift to slightly higher values for $[(TPP)Ru(NO)(H_2O)]^+$ (Figure S2, Table 2), as expected from the exchange of ethyl donors by electron-withdrawing phenyl groups in TPP. Accordingly, the second oxidation is no longer fully reversible for the TPP compound, which is also recognized from the spectroelectrochemical behavior. In contrast to the oxidations, even the first reduction of $[(Por)Ru(NO)(H_2O)]^+$ complexes was irreversible[7] and thus not investigated further. However, as reported earlier,[7] the addition of pyridine to solutions of $[(TPP)Ru(NO)(H_2O)]^+$ forms $[(TPP)Ru(NO)(py)]^+$ (Figure S1), which can be reversibly reduced at $E_{1/2}$(red1) = −0.79 V versus $Fc^{+/0}$. By varying the electronic effect of the pyridine by means of a substitution in the para position, we observed corresponding shifts of the potential for reduction (Table 2). A better electron acceptor than pyridine, 4-cyanopyridine, shifts the potential for the first reduction of $[(TPP)Ru(NO)(X)]^+$ to a less-negative value (−0.68 V versus $Fc^{+/0}$), whereas 4-*N,N*-dimethylaminopyridine, a better electron donor but poorer π-electron acceptor than unsubstituted pyridine, makes the complex more difficult to reduce by shifting the potential to a more negative value, −0.90 V versus $Fc^{+/0}$. A similar trend was observed for the reduction of $[(OEP)Ru(NO)(X)]^+$ with different pyridines (Table 2). The sites of the reversible electron-transfer processes, the two oxidations of $[(Por)Ru(NO)(H_2O)]^+$ and the reduction of $[(Por)Ru(NO)(X)]^+$, were determined by spectroelectrochemical measurements.

IR Spectroelectrochemistry. The accessibility of oxidized forms of $[(Por)Ru(NO)(H_2O)]^+$ and of the reduced forms of $[(Por)Ru(NO)(X)]^+$ allowed us to investigate the location of the redox processes by IR spectroelectrochemistry. Table 3 summarizes the data on the vibrational frequency of NO in different states together with DFT-calculated results. The oxidation of the aqua complexes causes comparatively small positive shifts of $\Delta\nu$(NO) = 27 and 18 cm^{-1} for $[(TPP)Ru(NO)(H_2O)]^{+/2+}$ and $[(OEP)Ru(NO)(H_2O)]^{+/2+}$, respectively, suggesting that the oxidation occurs on neither NO nor Ru but on the porphyrin ring (Figure 3, top). Similar shifts were noted for CO analogues.[9a] DFT calculations give a ca. 20 cm^{-1} positive shift of the NO stretching frequencies for both TPP and OEP complexes, which is in agreement with the experiments. Moreover, the appearance of porphyrin radical anion ("radical cation")[19] diagnostic ring vibrational bands[20] at 1531 cm^{-1} for $OEP^{\bullet-}$ and at 1290 cm^{-1} for $TPP^{\bullet-}$ after the spectroelectrochemical oxidation of the aqua complexes also confirms that the porphyrin ring is the target of the electron-transfer process of oxidation.[9,20] DFT calculations found intense, almost-degenerate pairs of ring vibration bands at 1548 and 1549 cm^{-1} or 1295 and 1298 cm^{-1} for the oxidized OMP or TPP complex, respectively.

The second oxidation causes a positive shift of $\Delta\nu$(NO) = 55 cm^{-1} for $[(OEP)Ru(NO)(H_2O)]^+$ in CH_2Cl_2/0.1 M n-Bu_4NClO_4 (Figure 3, middle). A high-energy shift of 64 cm^{-1} is also observed for the 1531 cm^{-1} ring vibrational band. $\Delta\nu$(NO) = 55 cm^{-1} may be compared to $\Delta\nu$(NO) = 79 cm^{-1} observed for the $Ru^{II} \rightarrow Ru^{III}$ transition in $[Ru(NO)Cl_5]^{(2-)\rightarrow(-)}$,[21e] suggesting the relevance of a presumably spin-paired $[(OEP^{\bullet-})Ru^{III}(NO^+)(H_2O)]^{3+}$ configuration as an

(19) One-electron oxidized porphyrins are often referred to as "radical cations" because they often contain coordinated metal dications. However, the ligands themselves are then oxidized from their normal dinegative forms, Por^{2-}, to radical anions, $Por^{\bullet-}$.

(20) Shimomura, E. T.; Phillippi, M. A.; Goff, H. M.; Scholz, W. F.; Reed, C. A. *J. Am. Chem. Soc.* **1981**, *103*, 6778.

Table 3. Experimental and G03/BPW91-Calculated NO Stretching Frequencies for $[(Por)Ru(NO)(X)]^{n+}$ Complexes

	$n = 2$		$n = 1$		$n = 0$	
	calcd. ν/cm^{-1}	exptl. ν/cm^{-1}	calcd. ν/cm^{-1}	exptl. ν/cm^{-1}	calcd. ν/cm^{-1}	exptl. ν/cm^{-1}
$[(TPP)Ru(NO)(H_2O)]^{n+}$	1922	1902	1904	1875		n.o.
$[(TPP)Ru(NO)(Py)]^{n+}$		n.o.	1903	1885	1665	1584
$[(OEP)Ru(NO)(H_2O)]^{n+}$	1921[a]	1895[b]	1901	1877		n.o.
$[(OEP)Ru(NO)(Py)]^{n+}$		n.o.	1901	1876	1664	1568

[a] 1941 cm^{-1} calculated for $n = 3$. [b] 1950 cm^{-1} observed for $n = 3$.

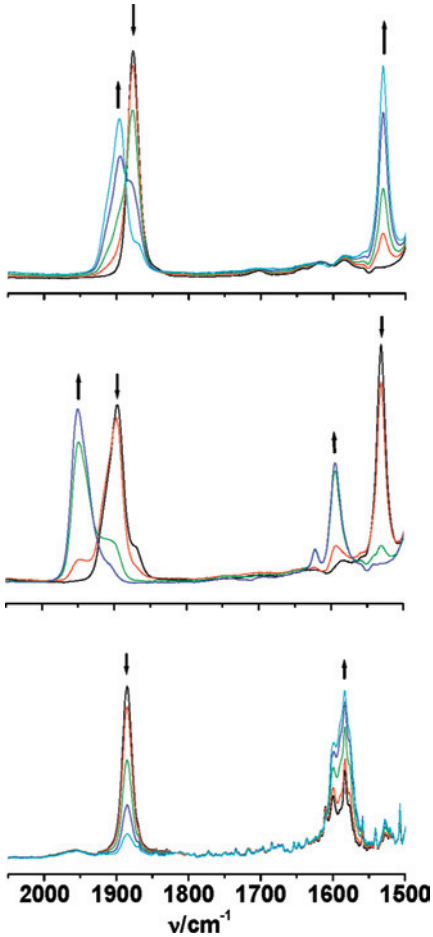

Figure 3. IR spectroelectrochemical response for the first oxidation (top) and second oxidation (middle) of $[(OEP)Ru(NO)(H_2O)]BF_4$ and for the reduction of $[(TPP)Ru(NO)(py)]BF_4$ (bottom) in CH_2Cl_2/0.1 M n-Bu_4NClO_4 at 298 K.

alternative to $[(OEP^{o})Ru^{II}(NO^{+})(H_2O)]^{3+}$. A corresponding claim was earlier made for systems $[(TPP)Ru(CO)(X)]^{2+}$.[9a] The combination of mono-oxidized porphyrin ligands with oxidized metal centers is of greater general interest with respect to active intermediates of heme enzymes (e.g., peroxidases);[22] $S = 0$ or 1 ground states can be considered but are difficult to distinguish, for instance, by EPR, when there is a lack of isolated material. Metal/porphyrin π overlap and thus partial covalency would result in shifts of both ν(NO) and of porphyrin ring vibrational bands. The DFT-calculated frontier orbitals for the lowest ^{3}A state of the model $[(OMP)Ru(NO)(H_2O)]^{3+}$ are shown in Figure S6. Although the singly occupied orbitals have OMP character, the energy difference between the SOMO and the almost-degenerate HOMOs is only 0.13 eV. The next triplet state, where electron density is partially delocalized over Ru and NO, is energetically close. Solvent effects and the influence of

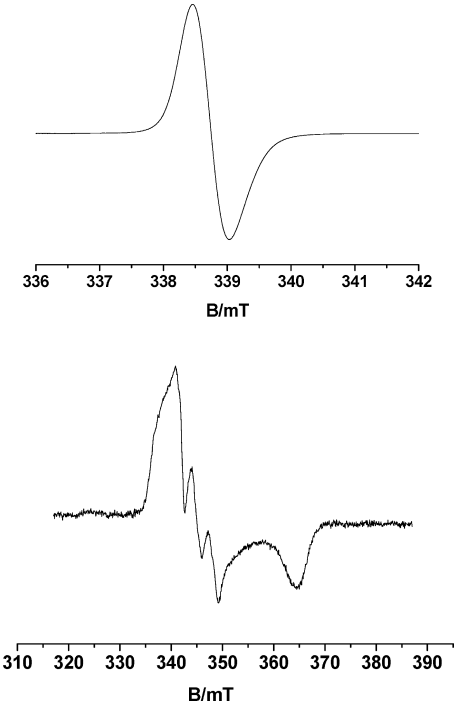

Figure 4. EPR spectrum of oxidized $[(OEP)Ru(NO)(H_2O)]BF_4$ (top, 298 K) and reduced $[(TPP)Ru(NO)(py)]BF_4$ (bottom, 110 K) in CH_2Cl_2/0.1 M n-Bu_4NClO_4.

counterions can change the relative energies of these close-lying states, possibly reversing their order.

The vibrational stretching band of NO shifts to lower values by a much larger amount (ca. -300 cm^{-1} for $[(Por)Ru(NO)(X)]^{+}$ during the reduction of the pyridine (X) complexes. Such large negative shifts in the vibrational frequency of NO are typical[21] for the reduction involving mainly electron uptake by nitrosyl-based orbitals (Figure 3, bottom). For both complexes, the DFT calculations indicate the formation of the typical bent Ru−N−O structure (Ru−N−O angle of 140.5° for both TPP and OMP complexes) during the reduction accompanied by negative shifts of the calculated NO-stretching frequencies by about 240 cm^{-1}.

(21) (a) Wanner, M.; Scheiring, T.; Kaim, W.; Slep, L. D.; Baraldo, L. M.; Olabe, J. A.; Záliš, S.; Baerends, E. J. *Inorg. Chem.* **2001**, *40*, 5704. (b) Sarkar, S.; Sarkar, B.; Chanda, N.; Kar, S.; Mobin, S. M.; Fiedler, J.; Kaim, W.; Lahiri, G. K. *Inorg. Chem.* **2005**, *44*, 6092. (c) Singh, P.; Sarkar, B.; Sieger, M.; Niemeyer, M.; Fiedler, J.; Záliš, S.; Kaim, W. *Inorg. Chem.* **2006**, *45*, 4602. (d) Videla, M.; Jacinto, J. S.; Baggio, R.; Garland, M. T.; Singh, P.; Kaim, W.; Slep, L. D.; Olabe, J. A. *Inorg. Chem.* **2006**, *45*, 8608. (e) Sieger, M.; Sarkar, B.; Záliš, S.; Fiedler, J.; Escola, N.; Doctorovich, F.; Olabe, J. A.; Kaim, W. *Dalton Trans.* **2004**, 1797.

(22) Kaim, W.; Schwederski, B. *Bioinorganic Chemistry: Inorganic Elements in the Chemistry of Life: An Introduction and Guide*; Wiley: Chichester, U.K., 1994.

Table 4. Experimental and Calculated EPR Parameters for $[(Por)Ru(NO)(X)]^0$

axial ligand (X)	g_{xx}	g_{yy}	g_{zz}	$A_{yy}(^{14}N)$/G
4-cyanopyridine	2.036 (TPP)	1.985 (TPP)	1.886 (TPP)	33 (TPP)
	2.009 (OEP)	1.986 (OEP)	1.881(OEP)	32 (OEP)
pyridine	2.036 (TPP)	1.985 (TPP)	1.880 (TPP)	33 (TPP)
	2.027 (TPP)[a]	1.983 (TPP)[a]	1.923 (TPP)[a]	31.8 (TPP)[a]
	2.002 (OEP)	1.984 (OEP)	1.877 (OEP)	32 (OEP)
	2.028 (OMP)[a]	1.984 (OMP)[a]	1.916 (OMP)[a]	31.8 (OMP)[a]
4-*N,N*-dimethylaminopyridine	2.036 (TPP)	1.985 (TPP)	1.878 (TPP)	33 (TPP)
	2.017 (OEP)	1.985 (OEP)	1.872 (OEP)	32 (OEP)

[a] Calculated values.

EPR Spectroelectrochemistry. EPR spectroscopy supports the above interpretations. The reversibly-obtained oxidized forms $[(Por)Ru(NO)(H_2O)]^{2+}$ show signals at $g_{iso} = 2.0002$ (TPP complex) and 2.0017 (OEP complex) and line widths of about 25 G (Figure 4, top; Figure S3). Such EPR signals with $g_{iso} \approx 2.00$ and without noticeable g anisotropy in the frozen state at X-band frequency (9.5 GHz) are typical for organic radicals and here for paramagnetic species containing the spin almost exclusively in the conjugated π system of the porphyrin ring.[9,23,24] Metal-based oxidation should result in rather large g anisotropy that is well detectable at X-band frequency and $g_{iso} > 2$ for a $4d^5$ (Ru^{III}) configuration because of the high SO coupling constant of Ru^{III};[21] thus, the formation of ruthenium(III) during the first oxidation can be excluded. No EPR signal was observed during the further oxidation to the (3^+) ion, which would be compatible with a singlet or rapidly-relaxing triplet species.

The EPR spectra of the obtained reduced species $[(Por)Ru(NO)(X)]^0$ (Figure 4, bottom; Table 4) show typically[11] invariant EPR characteristics (g factors $g_1 > 2$, $g_2 \approx 2.0$, $g_3 < 2$; $A_2(^{14}N) \approx 3.4$ mT) of $\{RuNO\}^7$ species that have been previously observed for a large number of very different complexes containing RuNO where the spin resides mainly (ca. 70%) on the NO ligand.[11] Figure 5 shows the difference between spin densities calculated for oxidized $[(TPP)Ru(NO)(H_2O)]^{2+}$ (spin density on porphyrin) and reduced [(TPP)Ru(NO)(py)] (spin density of 0.68 on the NO ligand). The DFT-calculated EPR parameters listed in Table 4 agree satisfactorily with the experimental data; the calculations confirm either porphyrin- or NO-centered processes in the course of the first oxidation or reduction, respectively (Tables 5 and 6).

DFT Calculations. The compositions of the DFT-calculated frontier orbitals of $[(TPP)Ru(NO)(H_2O)]^+$ and $[(TPP)Ru(NO)(py)]^+$ complexes are listed in Tables 5 and 6. The set of two almost-degenerate lowest-unoccupied molecular orbitals (LUMO and LUMO+1) is mainly formed by π^* orbitals of the NO ligand with contributing 4d (Ru) orbitals. Two closely lying highest-occupied orbitals (HOMO and HOMO−1) are mainly composed of π (porphyrin) orbitals. Pyridine and H_2O do not contribute substantially to the frontier orbitals; the most significant of such an effect concerns the LUMO of $[(TPP)Ru(NO)(py)]^+$ with a 4% contribution from pyridine. Accordingly, the stabilization of the reduced forms has been achieved with pyridine axial ligands.

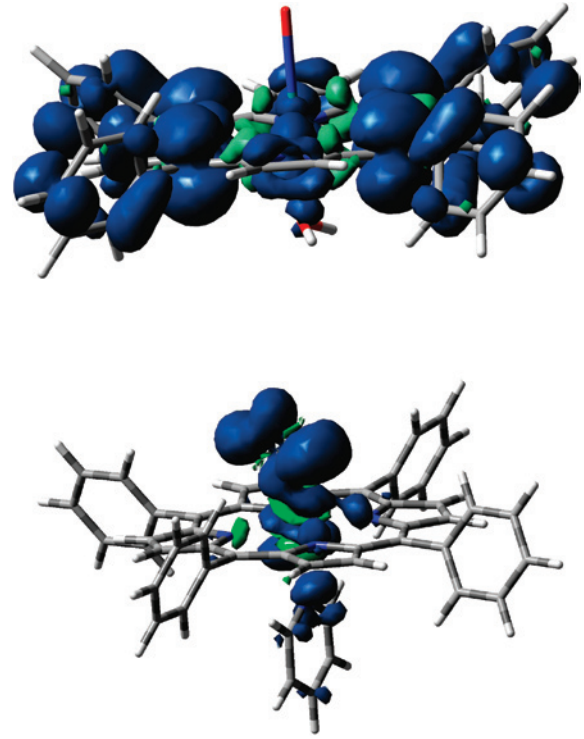

Figure 5. Representation of spin densities of $[(TPP)Ru(NO)(H_2O)]^{2+}$ (top) and [(TPP)Ru(NO)(py)] (bottom).

Table 5. DFT G03/PBE0-Calculated One-Electron Energies and Compositions of Selected Highest-Occupied and Lowest-Unoccupied Molecular Orbitals of the $[(TPP)Ru(NO)(H_2O)]^+$ Complex Expressed in Terms of Composing Fragments

MO	E (eV)	prevailing character	Ru	NO	porph	H_2O
		unoccupied				
LUMO+3	−4.91	π^* por + Ru	14	21	65	0
LUMO+2	−4.93	π^* por + Ru	14	21	64	0
LUMO+1	−5.37	π^* NO + Ru	15	45	40	0
LUMO	−5.40	π^* NO + Ru	15	47	38	0
		occupied				
HOMO	−8.17	π por	1	0	98	1
HOMO−1	−8.45	π por	0	0	100	0
HOMO−2	−9.27	π por	0	0	100	0
HOMO−3	−9.30	π por	0	0	100	0

Following theoretical and experimental results, especially the combined EPR and IR spectroelectrochemical measurements, we have thus established the sequence of oxidation state combinations, as shown in Scheme 1.

UV−Vis Spectroelectrochemistry. As known from a great amount of work on porphyrins and their metal

(23) (a) Wayland, B. B.; Newman, A. R. *Inorg. Chem.* **1981**, *20*, 3093. (b) Renner, M. W.; Cheng, R. J.; Chang, C. K.; Fajer, J. *J. Phys. Chem.* **1990**, *94*, 8508. (c) Tokita, Y.; Yamaguchi, K.; Watanabe, Y.; Morishima, I. *Inorg. Chem.* **1993**, *32*, 329. (d) Bhaskar, G.; Krishnan, V. *Inorg. Chem.* **1985**, *24*, 3253.

(24) Fuhrhop, J. H.; Kadish, K. M.; Davis, D. G. *J. Am. Chem. Soc.* **1973**, *95*, 5140.

Table 6. DFT G03/PBE0-Calculated One-Electron Energies and Compositions of Selected Highest-Occupied and Lowest-Unoccupied Molecular Orbitals of the $[(TPP)Ru(NO)(py)]^+$ Complex Expressed in Terms of Composing Fragments

MO	E (eV)	prevailing character	Ru	NO	porph	py
		unoccupied				
LUMO+3	−4.80	π^* por + Ru	11	15	73	0
LUMO+2	−4.82	π^* por + Ru	10	12	77	2
LUMO+1	−5.30	π^* NO + Ru	17	52	30	1
LUMO	−5.32	π^* NO + Ru	17	53	25	4
		occupied				
HOMO	−7.98	π por	1	0	98	1
HOMO−1	−8.27	π por	0	0	100	0
HOMO−2	−9.17	π por	0	0	100	0
HOMO−3	−9.18	π por	0	0	100	0

Scheme 1

$[(Por^{\bullet-})Ru^{III}(NO^+)(X)]^{3+}$

$\overset{-e^-}{\rightleftharpoons}\overset{+e^-}{}$

$[(Por^{\bullet-})Ru^{II}(NO^+)(X)]^{2+}$ X = H_2O

$\overset{-e^-}{\rightleftharpoons}\overset{+e^-}{}$ ↑ oxidation

$[(Por^{2-})Ru^{II}(NO^+)(X)]^+$ X = H_2O, pyridines

$\overset{-e^-}{\rightleftharpoons}\overset{+e^-}{}$ ↓ reduction

$[(Por^{2-})Ru^{II}(NO^{\bullet})(X)]^0$ X = pyridines

Por = TPP, OEP

complexes,[5,9] the UV−vis absorption spectra of ruthenium nitrosyl porphyrins show blue-shifted Q bands and a very sharp Soret band (Table 7). As illustrated in Figure 6, the spectrum of oxidized $[(TPP)Ru(NO)(H_2O)]^{(+)\rightarrow(2+)}$ displays a decrease in the intensity of both the Soret and the Q band. Whereas the Soret band is only partially diminished, the Q band at 558 nm seems to disappear completely at the cost of new broad bands at 616, 658, and 742 nm. Such change in absorption spectra is typical[5,9] for the formation of porphyrin π-radical complexes. During the second oxidation, there is a noticeable splitting of the Soret band in the UV region, and the transitions in the visible are diminished (Figure S4).

The splitting of the Soret band observed particularly after the two-electron oxidation of $[(TPP)Ru(NO)(H_2O)]^+$ and in

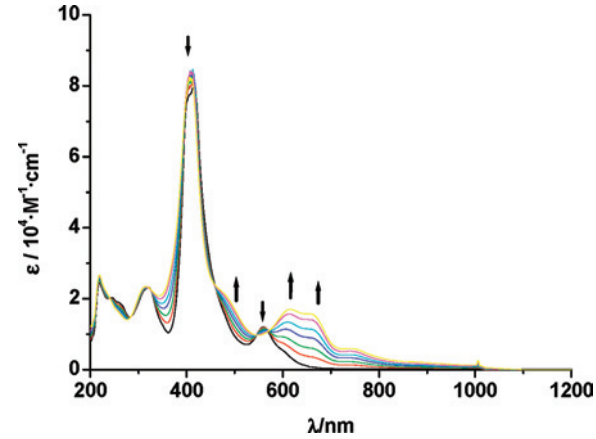

Figure 6. UV−vis spectroelectrochemical response for the conversion $[(TPP)Ru(NO)(H_2O)]^{(+)\rightarrow(2+)}$ in CH_2Cl_2/0.1 M n-Bu_4NClO_4.

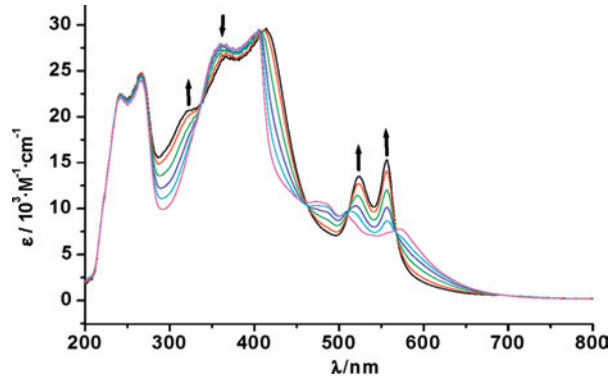

Figure 7. UV−vis spectroelectrochemical response for the conversion $[(OEP)Ru(NO)(py)]^{(+)\rightarrow(0)}$ in CH_2Cl_2/0.1 M n-Bu_4NClO_4.

the spectra of the OEP complex presumably arises from perturbed orbital degeneracy when the ligand arrangement induces a lower-than-D_{4h} symmetry (e.g., through different axial ligands); such Soret and Q-band splitting has been observed before.[25]

In contrast, the UV−vis spectroelectrochemical reduction experiments for $[(Por)Ru(NO)(py)]^+$ (Por = OEP, Figure 7; Por = TPP, Figure S5) show a nitrosyl-based reduction[7,11,21] accompanied by the appearance of new bands in the visible region (Table 7); these could be due to metal-to-ligand charge transfer (MLCT) transitions d(Ru) → $\pi^*(NO^{\bullet})$ and to ligand-to-ligand charge transfer processes $\pi^*(NO^{\bullet}) \rightarrow \pi^*$(Por).

The assignments are in agreement with the calculated molecular orbital scheme (Table 6). In the reduced complex, an excitation of the unpaired electron from an orbital with

Table 7. Absorption Data and TD-DFT-Calculated Lowest-Lying Transitions for Porphyrin Complexes

compounds	λ/nm (ε/$M^{-1}\cdot cm^{-1}$)[a]
$[(TPP)Ru(NO)(H_2O)]^+$ (exp) (TD-DFT-calculated)	410 (78 000), 558 (12 000) 391 (1.248), 391 (1.228), 482 (0.065), 483 (0.068), 610 (0.026), 621 (0.029)
$[(TPP)Ru(NO)(H_2O)]^{2+}$	408 (84 000), 496 (sh), 616 (17 000), 658 (15 700), 742(5900)
$[(TPP)Ru(NO)(py)]^+$ (TD-DFT-calculated)	278, 324, 400, 422, 492, 540, 573, 620 326 (0.187), 396 (1.197), 397 (1.125), 501 (0.056), 503 (0.055), 674 (0.016), 679 (0.016)
$[(TPP)Ru(NO)(py)]^0$	279, 310, 394, 430, 538, 574
$[(OEP)Ru(NO)(H_2O)]^+$	370 (40 600), 397 (42 400), 478 (11 000)
$[(OEP)Ru(NO)(H_2O)]^{2+}$	488 (11 500), 574 (89 800), 642 (62 400)
$[(OEP)Ru(NO)(py)]^+$	266, 359, 484, 507, 573
$[(OEP)Ru(NO)(py)]^0$	319, 362, 524, 557

[a] Calculated values: λ in nanometers (oscillator strengths).

prevailing contributions from Ru and NO (labeled LUMO or LUMO+1 in Table 6) is considered to lead to a mainly π^*(porphyrin)-based level (LUMO+2 or LUMO+3).

Conclusions

We have observed the reversible electron-transfer processes for ruthenium nitrosyl porphyrins by varying the axial ligand. Except for the redox potentials, the differences among complexes involving different pyridine ligands have been small. The complexes of the type $[(Por)Ru(NO)(X)]BF_4$ containing X as a neutral O-donor aqua ligand show a two-step oxidation, and those with X as a neutral N-donor pyridine ligand show a reversible reduction. The sites of all processes have been assessed by means of IR and UV−vis−NIR spectroelectrochemical measurements and through theoretical support. The first oxidation of $[(Por)Ru(NO)(H_2O)]^+$ occurs on the porphyrin ring, as documented now completely by EPR, IR, and UV−vis−NIR spectroelectrochemistry. This is then followed by a metal involving second oxidation according to the observed $\Delta\nu$ (NO) shift. That species is EPR silent, and its further calculations and, if possible, NMR spectroscopic investigation, are warranted. The reduction of $[(Por)Ru(NO)(Py)]^+$ is mainly NO-centered, as established spectroelectrochemically by EPR and IR and as noted similarly for many other $\{RuNO\}^{6,7}$ systems.[11] Thus, we have shown that EPR gives clear answers for the spin location, except for the EPR-silent and still puzzling tricationic form, that IR spectroelectrochemistry reveals charge effects at NO and in some cases at the porphyrins, and that the characterized oxidation state distributions cause electronic absorption features that may be useful for future studies. The fascinating metal/NO interaction relevant to biochemistry,[26] organic chemistry,[27] and catalysis[28] can thus be probed via an array of spectroelectrochemical methods, including EPR.

Acknowledgment. This work has been supported by the Deutsche Forschungsgemeinschaft (Graduate College "Magnetic Resonance" and project Ka 618/27-1), by the European Union (COST D35), by the Grant Agency of the Academy of Sciences of the Czech Republic (KAN100400702) and the Ministry of Education of the Czech Republic (OC 139), and by Argentinian grants PICT 03/14418 and X104 from the ANPCYT and the UBA, respectively.

Supporting Information Available: X-ray crystallographic file for $[(TPP)Ru(NO)(H_2O)]BF_4$; Experimental and calculated structure parameters for $[(TPP)Ru(NO)(H_2O)]^+$); IR spectroelectrochemical response of $[(TPP)Ru(NO)(H_2O)]BF_4$ with 10-fold excess of pyridine; cyclic voltammogram of $[(TPP)Ru(NO)(H_2O)]BF_4$; EPR spectrum of $[(TPP)Ru(NO)(H_2O)]^{2+}$; UV−vis spectroelectrochemical response for the conversion $[(OEP)Ru(NO)(H_2O)]^{(2+)\rightarrow(3+)}$; UV−vis spectroelectrochemical response for the conversion $[(TPP)Ru(NO)(Py)]^{(+)\rightarrow(0)}$; and frontier orbitals of $[(OMP)Ru(NO)(H_2O)]^{3+}$). This material is available free of charge via the Internet at http://pubs.acs.org.

IC702371T

(25) (a) Jansen, G.; Noort, M. *Spectrochim. Acta* **1976**, *32A*, 747. (b) Canters, C. W.; van der Waals, J. H.; High Resolution Zeeman Spectroscopy of Metalloporphyrins. In *The Porphyrins*; Dolphin, D., Ed.; Academic Press: New York, 1978; *Vol. 3*, p. 531. (c) Suisalu, A.; Mauring, K.; Kikas, J.; Herenyi, L.; Fidy, J. *Biophys. J.* **2001**, *80*, 498.

(26) Ghosh, A. *Acc. Chem. Res.* **2005**, *38*, 943.

(27) (a) Di Salvo, F.; Escola, N.; Scherlis, D. A.; Estrin, D. A.; Bondía, C.; Murgida, D.; Ramallo-López, J. M.; Requejo, F. G.; Shimon, L.; Doctorovich, F. *Chem.−Eur. J.* **2007**, *13*, 8428. (b) Doctorovich, F.; Di Salvo, F. *Acc. Chem. Res.* **2007**, *40*, 985.

(28) Hong, S.; Rahman, T. S.; Jacobi, K.; Ertl, G. *J. Phys. Chem. C* **2007**, *111*, 12361.